



# Open-source do-it-yourself multi-color fluorescence smartphone microscopy

YULUNG SUNG,<sup>1</sup> FERNANDO CAMPA,<sup>1</sup> AND WEI-CHUAN SHIH<sup>1,2,3,4,\*</sup>

<sup>1</sup>Department of Electrical & Computer Engineering, University of Houston, 4800 Calhoun Rd, Houston, TX 77204, USA

<sup>2</sup>Department of Biomedical Engineering, University of Houston, Houston, TX 77204, USA

<sup>3</sup>Program of Materials Science & Engineering, University of Houston, Houston, TX 77204, USA

<sup>4</sup>Department of Chemistry, University of Houston, Houston, TX 77204, USA

\*wshih@uh.edu

**Abstract:** Fluorescence microscopy is an important technique for cellular and microbiological investigations. Translating this technique onto a smartphone can enable particularly powerful applications such as on-site analysis, on-demand monitoring, and point-of-care diagnostics. Current fluorescence smartphone microscope setups require precise illumination and imaging alignment which altogether limit its broad adoption. We report a multi-color fluorescence smartphone microscope with a single contact lens-like add-on lens and slide-launched total-internal-reflection guided illumination for three common tasks in investigative fluorescence microscopy: autofluorescence, fluorescent stains, and immunofluorescence. The open-source, simple and cost-effective design has the potential for do-it-yourself fluorescence smartphone microscopy.

© 2017 Optical Society of America

**OCIS codes:** (110.0180) Microscopy; (180.2520) Fluorescence microscopy; (260.6970) Total internal reflection; (120.3620) Lens system design; (100.1455) Blind deconvolution.

## References and links

1. J. W. Lichtman and J. A. Conchello, "Fluorescence microscopy," *Nat. Methods* **2**(12), 910–919 (2005).
2. S. Rahman and J. Lipert, "Exploration of simple analytical approaches for rapid detection of pathogenic bacteria," Iowa State University (2005).
3. I. Pavlova, M. Williams, A. El-Naggar, R. Richards-Kortum, and A. Gillenwater, "Understanding the biological basis of autofluorescence imaging for oral cancer detection: high-resolution fluorescence microscopy in viable tissue," *Clin. Cancer Res.* **14**(8), 2396–2404 (2008).
4. B. N. Giepmans, S. R. Adams, M. H. Ellisman, and R. Y. Tsien, "The fluorescent toolbox for assessing protein location and function," *Science* **312**(5771), 217–224 (2006).
5. R. Yuste, "Fluorescence microscopy today," *Nat. Methods* **2**(12), 902–904 (2005).
6. P. Mandal, A. Biswas, K. Choi, and U. Pal, "Methods for rapid detection of foodborne pathogens: an overview," *Am. J. Food Technol.* **6**, 87–102 (2011).
7. F. Kawamoto, "Rapid diagnosis of malaria by fluorescence microscopy with light microscope and interference filter," *Lancet* **337**(8735), 200–202 (1991).
8. W. W. Franke, E. Schmid, M. Osborn, and K. Weber, "Different intermediate-sized filaments distinguished by immunofluorescence microscopy," *Proc. Natl. Acad. Sci. U.S.A.* **75**(10), 5034–5038 (1978).
9. L. Shen, J. A. Hagen, and I. Papautsky, "Point-of-care colorimetric detection with a smartphone," *Lab Chip* **12**(21), 4240–4243 (2012).
10. K. Doi, "Current status and future potential of computer-aided diagnosis in medical imaging," *Br. J. Radiol.* **78**, s3–s19 (2005).
11. A. R. Miller, G. L. Davis, Z. M. Oden, M. R. Razavi, A. Fateh, M. Ghazanfari, F. Abdolrahimi, S. Poorazar, F. Sakhaie, R. J. Olsen, A. R. Bahrmand, M. C. Pierce, E. A. Graviss, and R. Richards-Kortum, "Portable, battery-operated, low-cost, bright field and fluorescence microscope," *PLoS One* **5**(8), e11890 (2010).
12. K. K. Ghosh, L. D. Burns, E. D. Cocker, A. Nimmerjahn, Y. Ziv, A. E. Gamal, and M. J. Schnitzer, "Miniaturized integration of a fluorescence microscope," *Nat. Methods* **8**(10), 871–878 (2011).
13. S. Battiatto and M. Moltisanti, "The future of consumer cameras," *Proceedings of the SPIE*, 93990C (2015).
14. S. Kulkarni and P. Agrawal, "Smartphone driven healthcare system for rural communities in developing countries," in *Proceedings of the 2nd international workshop on systems and networking support for health care and assisted living environments(ACM2008)*, p. 8.
15. X. Xu, A. Akay, H. Wei, S. Wang, B. Pinguang-Murphy, B. E. Erlandsson, X. Li, W. Lee, J. Hu, and L. Wang, "Advances in smartphone-based point-of-care diagnostics," *Proc. IEEE* **103**, 236–247 (2015).

16. C. Gurrin, Z. Qiu, M. Hughes, N. Caprani, A. R. Doherty, S. E. Hodges, and A. F. Smeaton, "The smartphone as a platform for wearable cameras in health research," *Am. J. Prev. Med.* **44**(3), 308–313 (2013).
17. F. Snik, J. H. Rietjens, A. Aputuley, H. Volten, B. Mijling, A. Di Noia, S. Heikamp, R. C. Heinsbroek, O. P. Hasekamp, and J. M. Smit, "Mapping atmospheric aerosols with a citizen science network of smartphone spectropolarimeters," *Geophys. Res. Lett.* **41**, 7351–7358 (2014).
18. D. N. Breslauer, R. N. Maamari, N. A. Switz, W. A. Lam, and D. A. Fletcher, "Mobile phone based clinical microscopy for global health applications," *PLoS One* **4**(7), e6320 (2009).
19. Q. Wei, H. Qi, W. Luo, D. Tseng, S. J. Ki, Z. Wan, Z. Göröcs, L. A. Bentolila, T. T. Wu, R. Sun, and A. Ozcan, "Fluorescent imaging of single nanoparticles and viruses on a smart phone," *ACS Nano* **7**(10), 9147–9155 (2013).
20. H. C. Koydemir, Z. Gorocs, D. Tseng, B. Cortazar, S. Feng, R. Y. L. Chan, J. Burbano, E. McLeod, and A. Ozcan, "Rapid imaging, detection and quantification of *Giardia lamblia* cysts using mobile-phone based fluorescent microscopy and machine learning," *Lab Chip* **15**(5), 1284–1293 (2015).
21. Z. F. Phillips, M. V. D'Ambrosio, L. Tian, J. J. Rulison, H. S. Patel, N. Sadras, A. V. Gande, N. A. Switz, D. A. Fletcher, and L. Waller, "Multi-contrast imaging and digital refocusing on a mobile microscope with a domed led array," *PLoS One* **10**(5), e0124938 (2015).
22. Y. L. Sung, J. Jeang, C. H. Lee, and W. C. Shih, "Fabricating optical lenses by inkjet printing and heat-assisted in situ curing of polydimethylsiloxane for smartphone microscopy," *J. Biomed. Opt.* **20**(4), 047005 (2015).
23. Y. L. Sung, J. Garan, H. Nguyen, Z. Hu, and W.-C. Shih, "Automated batch characterization of inkjet-printed elastomer lenses using a LEGO platform," *Appl. Opt.* **56**, 7346–7350 (2017).
24. Y. L. Sung, F. Campa, and W. C. Shih, "3D design files for smartphone fluorescence microscopy," <https://doi.org/10.6084/m9.figshare.5313643> figshare (2017).
25. J. S. Ploem, "The use of a vertical illuminator with interchangeable dichroic mirrors for fluorescence microscopy with incidental light," *Z. Wiss. Mikrosk.* **68**(3), 129–142 (1967).
26. B. N. Kim, J. A. Diaz, S. G. Hong, S. H. Lee, and L. P. Lee, "Dark-field smartphone microscope with nanoscale resolution for molecular diagnostics," in *MicroTAS(2014)*, pp. 2247–2249.
27. H. Zhu, O. Yaglidere, T. W. Su, D. Tseng, and A. Ozcan, "Cost-effective and compact wide-field fluorescent imaging on a cell-phone," *Lab Chip* **11**(2), 315–322 (2011).
28. L. Boulos, M. Prévost, B. Barbeau, J. Coallier, and R. Desjardins, "LIVE/DEAD® BacLight™ : application of a new rapid staining method for direct enumeration of viable and total bacteria in drinking water," *J. Microbiol. Methods* **37**(1), 77–86 (1999).
29. P. J. De Temmerman, E. Verleysen, J. Lammertyn, and J. Mast, "Semi-automatic size measurement of primary particles in aggregated nanomaterials by transmission electron microscopy," *Powder Technol.* **261**, 191–200 (2014).
30. H. B. Glasgow, J. M. Burkholder, R. E. Reed, A. J. Lewitus, and J. E. Kleinman, "Real-time remote monitoring of water quality: a review of current applications, and advancements in sensor, telemetry, and computing technologies," *J. Exp. Mar. Biol. Ecol.* **300**, 409–448 (2004).
31. G. Leedale, B. Meeuse, and E. Pringsheim, "Structure and physiology of *Euglena spirogyra*. I and II," *Arch. Microbiol.* **50**, 68–102 (1965).
32. R. Porra, W. Thompson, and P. Kriedemann, "Determination of accurate extinction coefficients and simultaneous equations for assaying chlorophylls a and b extracted with four different solvents: verification of the concentration of chlorophyll standards by atomic absorption spectroscopy," *BBA* **975**, 384–394 (1989).
33. D. Pittet, S. Dharan, S. Touveneau, V. Sauvan, and T. V. Perneger, "Bacterial contamination of the hands of hospital staff during routine patient care," *Arch. Intern. Med.* **159**(8), 821–826 (1999).
34. J. C. Tiller, C. J. Liao, K. Lewis, and A. M. Klibanov, "Designing surfaces that kill bacteria on contact," *Proc. Natl. Acad. Sci. U.S.A.* **98**(11), 5981–5985 (2001).
35. R. D. Adam, "Biology of *Giardia lamblia*," *Clin. Microbiol. Rev.* **14**(3), 447–475 (2001).
36. C. L. DiGiorgio, D. A. Gonzalez, and C. C. Huitt, "Cryptosporidium and *Giardia* recoveries in natural waters by using environmental protection agency method 1623," *Appl. Environ. Microbiol.* **68**(12), 5952–5955 (2002).

## 1. Introduction

Fluorescence imaging is an indispensable technique for cellular and molecular identification [1–3], study of microbiological processes [4, 5], and rapid diagnosis [6, 7]. Fluorescence images can be acquired from endogenous or exogenous fluorophores that encode molecular specificity. In the former case, naturally-occurring molecular species such as tryptophan and chlorophyll can be imaged. In others, a vast library of artificial fluorophores can be employed to label targets by various binding chemistry or immunochemistry [8]. The demand for on-site analysis, on-demand monitoring, and point-of-care diagnosis [9, 10] have highlighted the need to create robust, portable, low-cost and simple-to-use fluorescence microscopes with on-board image processing or wireless communication capabilities, in order to extend the lab-based technique to regions without lab facilities or skilled personnel [11, 12].

Building additional functions on a smartphone is appealing due to their sheer adopted quantity. Globally, the 3 billion smartphone subscriptions in place today are projected to grow to 6 billion by 2020 [13] with major growth expected in the developing world. Similar to how mobile phone adoption bypassed the use of landline telephones in these regions, smartphone-based measurements can well replace traditional lab-based measurements [14]. The integration of smartphones into many daily routines makes it highly convenient, cost-effective, and powerful to develop new technologies on top of the platform with simple add-on accessories [15]. The readily available sensors, computational power, and wireless transmission capability [16], and the synergy between local and cloud computation and data storage have generated significant interest in telemedicine, global health, mobile sensor network, and citizen science [17].

To date, several microscopy imaging modalities and contrast mechanisms have been demonstrated on smartphone platforms: these include bright-field [18], oblique-angle fluorescence [19], epi-fluorescence [20], and phase-contrast [21]. In particular, increasingly powerful smartphone cameras have promoted the implementation of microscopic imaging with simple add-on lenses [22, 23]. However, the precise illumination and accurate optical alignment for fluorescence microscopy setups are quite challenging for a non-technical person to duplicate. Therefore, further development in smartphone microscopy platforms as well as applications are limited to an underwhelming number of research groups. To pursue ultra-simplicity for open-source do-it-yourself fluorescence smartphone microscopy, we report the development of an integrated single lens add-on for multi-color fluorescence imaging, and demonstrate its applications in various microbiological investigations. Designs can be downloaded from [Dataset 1](#) (Ref [24]), freely-modified, and printed with a 3D printer.

## 2. Setup

Epi-fluorescence is a dominant configuration in lab-based fluorescence microscopes, its performance critically depends on the quality of optical filters and objective lenses that incur significant cost [25]. The use of a condenser or objective lens poses another challenge with the thin and lightweight requirements of a smartphone microscope. Furthermore, many current portable fluorescence microscopy setups rely on directional LED illumination which require physical repositioning when used with lenses of different optical powers.

To overcome these limitations, we used orthogonal illumination and collection optical paths with decoupled designs [26, 27]. In other words, no adjustment is needed on the illumination side for different lenses or emission filters. The optical path is shown in Fig. 1(a). The excitation light is launched by light-emitting-diodes (LED) directly mounted on the side of a standard glass slide, providing illumination guided by total internal reflection (TIR) between the top and bottom glass / air interfaces. Illumination can be coupled out by the specimen in contact with the glass surface for exciting fluorescence which is collected by an inkjet-printed polymer lens [22] attached in front of a smartphone camera for imaging. The polymer lens self-adheres to any camera cover glass without supporting structures and is essentially alignment-free besides rough centering. The receptacle was designed to accommodate a standard 1 inch x 3 inch glass slide and five surface-mounted diode LEDs (5 mm x 5 mm). The critical angle for TIR at the glass / air interface by this launching geometry ranges from  $41.01^\circ$  ( $\lambda = 465$  nm, BK7 glass) to  $41.30^\circ$  ( $\lambda = 630$  nm). In other words, LED illumination with incidence half-angle  $< 48.8^\circ$  can be TIR-guided. Additional photometric measurements suggest ~95% of the coupled light lies within this angle. LEDs of different wavelengths are readily available as excitation illumination, and long-pass color filters were used as emission filters to block elastically scattered photons while allow fluorescence emission to pass through.

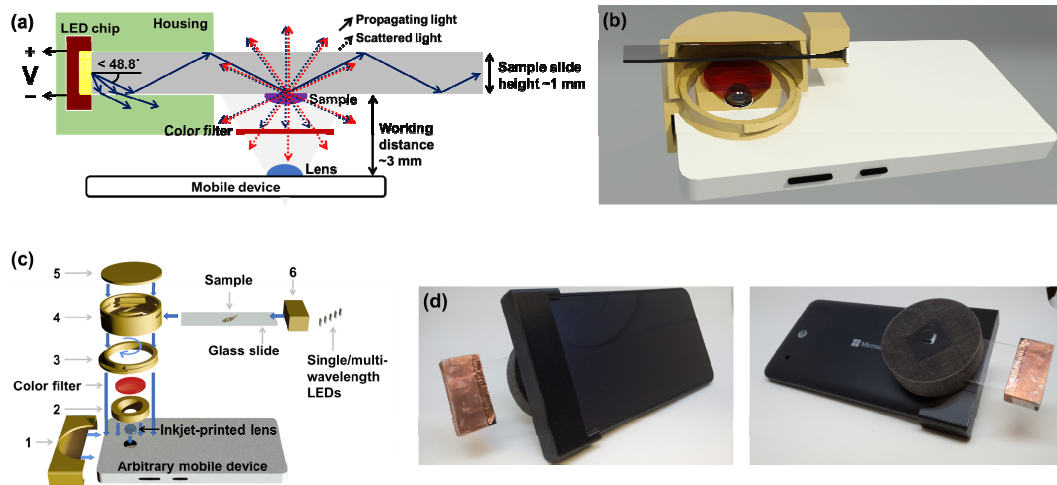


Fig. 1. (a) Slide-launched TIR-guided illumination: elastically scattered photons are blocked by the filter, while fluorescent photons can reach the smartphone camera. (b) Photorealistic cut-out rendering (c) Assembly procedure: inkjet-printed lens attached onto smartphone camera, smartphone adapter (1) fitted on smartphone, adhesive ring (2) attached to remove stray light, color filter attached on adhesive ring for fluorescence imaging, base ring (3) attached to adapter, threaded barrel (4) with slot enabled z-axis focusing and sample insertion, lid (5) attached to block ambient light, LED module (6) provided illumination. (d) System attached to smartphone.

Figure 1(b) and 1(c) shows parts designed in CAD software, and printed with polylactic-acid (PLA) by a desktop fused-filament 3D printer (Ultimaker 2+). The housing was assembled in the following order: 1) A phone adapter was attached to the smartphone. (2) A light blocking ring was attached to the smartphone to reduce stray light while accommodating a color filter. (3) A base ring was slotted into the adapter. (4) A threaded barrel with rectangular slits facing each other on the rim for the insertion of a sample glass slide. Opposing threads on the base ring and barrel enabled z-direction focusing of  $30\ \mu\text{m}$  per 1-degree rotation. Internal structures were designed to reduce stray light. (5) A lid was attached to block ambient light. (6) An illumination module with LEDs powered by LR44 batteries was attached to the glass slide for illumination. An inkjet-printed polymer lens was attached to the camera for image magnification. The design files are available from [Dataset 1](#) (Ref [24]).

The modular design enables different usage scenarios such as: imaging with an arbitrary smartphone by modifying the phone adapter; allowing different sample geometries by modifying the sample receptacle; and enabling backlit bright-field microscopy with the lid removed and without the LED attachment. Furthermore, the LEDs can be positioned and selected to achieve spatial and spectral multiplexing, and the combination of LED emission wavelength and color filter cut-on wavelength can be individually selected for different fluorescence applications, as illustrated in Fig. 1. The fluorescence microscope attachment on a smartphone (Lumia 640) is shown in Fig. 1(d). By using low-power LEDs, the attachment can operate on two 1.5V button batteries optimally for 1 hour. The entire attachment weighs 26.5 g including batteries, and costs less than \$20.

### 2.1 Phone selection and image capture and processing technique

An entry-level smartphone was used (Lumia 640, Microsoft). The phone was equipped with a 1/4-inch (5.08 mm X 3.81 mm), 8-megapixel (3264 x 2448 pixels) image sensor with a 4:3 crop ratio coupled to an  $f/2.2$  aperture lens. Focus was fixed to minimum working distance, master gain was minimized for improved signal-to-noise ratio and color accuracy, and shutter

speed was tuned for optimized visibility of dark features without saturation. Images were stored in RAW format which comprised the original Bayer pattern, and converted in-phone to uncompressed DNG format via RAW-to-DNG converter (Microsoft). Camera RAW plug-in for Photoshop (Adobe) was used to decode DNG images to lossless TIFF format for viewing and processing on a computer.

Blind deconvolution with a Gaussian point-spread-function was used to deblur the image and improve image quality. Specifically, we used the 'deconv' function in MATLAB (Mathworks) to deconvolve the original image using the maximum likelihood algorithm, assuming a Gaussian point-spread-function with a diameter that depended on the lens magnification and certain prior knowledge about the feature size.

## 2.2 Lens selection and focusing

We used low-cost inkjet-printed lenses that can be fabricated and characterized [22, 23]. The lens is self-adhesive to the smartphone, which greatly simplifies the design of other components. The focal length of the lens can be selected to optimally match the desired resolution or field-of-view (FOV). Here we used two lenses (high-res and low-res). The high-res lens was used to obtain images in Fig. 4, Fig. 6, and Fig. 8 for improved resolution of 2  $\mu\text{m}$  at the expense of decreased FOV, while the low-res lens was used for images in Fig. 5, Fig. 7, and Fig. 9.

The high-res lens has a focal length ( $f$ ) of 3 mm, which enables a minimum working distance (WD) of 3 mm when attached to the smartphone camera. The effective numerical aperture (NA) of the system is 0.15, yielding diffraction-limited resolution ( $R_{diff} = \lambda / 2NA$ ) of 1.6  $\mu\text{m}$ . Experimentally, this lens yielded a usable FOV of 2 x 2 mm<sup>2</sup> which is imaged by the center 1600 x 1600 pixels within the 3264 x 2448 pixels camera sensor, yielding a sampling resolution ( $R_{samp}$ ) of 1.25  $\mu\text{m}/\text{pixel}$ . The actual achievable resolution was experimentally obtained to be 2  $\mu\text{m}$  by imaging polystyrene beads. These images are directly comparable to those obtained with a desktop epi-fluorescence microscope with a 5x objective lens and 10x eyepiece. The low-res lens features  $f = 6$  mm. When attached to the smartphone camera, it enables WD = 5 mm, NA = 0.1,  $R_{diff} = 2.5$   $\mu\text{m}$ , FOV = 4 x 4 mm<sup>2</sup>, and  $R_{samp} = 2.5$   $\mu\text{m}$ . The achievable resolution was experimentally obtained to be 4  $\mu\text{m}$  by imaging polystyrene beads. We note that the achievable resolution depends on the externally attached lens, the crop factor of the smartphone camera, and the pixel density and size of the sensor. Better resolution can likely be obtained with newer smartphone models.

To ensure a properly focused image, rough focusing was performed by rotating the 3D printed barrel. The large size of the barrel enabled manual rotation intervals of 1-degree, equivalent to a 30  $\mu\text{m}$  z-direction movement. Fine focusing was performed by zooming into the live preview image and adjusting the smartphone lens stack to sensor distance through software.

## 2.3 LED and filter specifications

The LED (Epistar) selections and wavelengths are: UV ( $\lambda = 390$  nm, RL5-UV0315-380), Blue ( $\lambda = 465$  nm, 5050-B1200), Green ( $\lambda = 520$  nm, 5050-G3500), Yellow ( $\lambda = 590$  nm, 5050-Y1200), Red ( $\lambda = 630$  nm, 5050-R1200), and broadband white (6500k equivalent, 5050-PW6000). As shown in Fig. 2, spectra obtained experimentally deviate from specifications by up to 10 nm, and full-width at half-maximum was measured to be between 15 nm (UV) to 45 nm (green). Although the excitation illumination is broadband, by using widely separated fluorescence excitation / emission wavelengths, excitation filters are not needed. Long-pass color filters (Edmund Optics) were used with cut-on wavelengths at 400, 450, 525, 575, 625, and 675 nm.

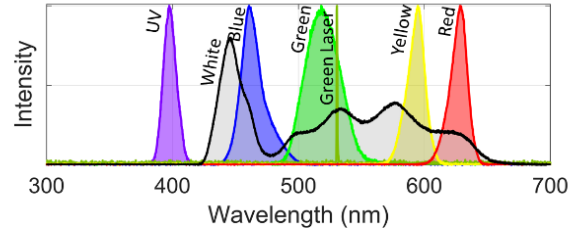


Fig. 2. Experimentally measured LED emission response show broad but well-defined peaks. Green laser from frequency-doubled Nd:YAG laser for comparison of spectral width.

#### 2.4 Illumination and filter selection for different fluorescence dyes

Proper selection of LED wavelength ( $\lambda_{LED}$ ) and cut-on filter wavelength ( $\lambda_{CUT-ON}$ ) to match fluorescence excitation / emission response is key to good image quality. For an arbitrary fluorescent molecule with excitation wavelength ( $\lambda_{ex}$ ) and emission wavelength ( $\lambda_{em}$ ), the LED with the nearest wavelength response ( $\lambda_{LED}$ ) to  $\lambda_{ex}$  was selected and paired with the long-pass filter with a cut-on wavelength ( $\lambda_{CUT-ON}$ ) slightly shorter than  $\lambda_{em}$  for the best results. Figure 3 provides the fluorescence excitation and emission wavelengths (solid lines), LED illumination spectral distribution (patch) and color-filter cut-on wavelength (dotted line) for fluorescence dyes used in this study.

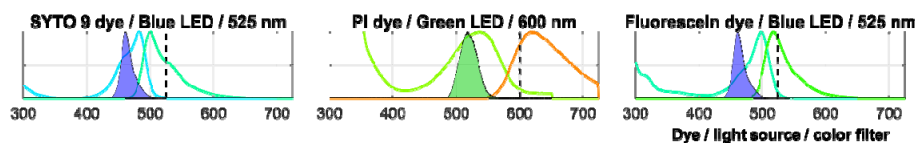


Fig. 3. Dyes used in this study and their respective fluorescence excitation / emission wavelength (solid lines), LED illumination response (patch) and color-filter cut-on wavelength (dotted line).

#### 2.5 Desktop fluorescence microscope for comparison

Desktop fluorescence microscope images were taken with an Olympus BX-51 fluorescence microscope equipped with a DP72 digital camera and two filter cubes: Fluorescein isothiocyanate (FITC) filter (ex/em: 495 / 519 nm) and Tetramethylrhodamine-Isothiocyanate (TRITC) filter (ex/em: 552 / 577 nm).

#### 2.6 Sample preparation and staining

Multi-color fluorescent polystyrene beads (T7283, ThermoFisher) were diluted with DI water and dried on a glass slide to produce regions of sparse single particles.

Gram-negative bacteria (*Escherichia coli* MG 1655) was prepared fresh from a single colony of tryptic soy agar plate in tryptic soy broth (TSA, TSB, Oxoid). The growth was carried out at 35°C with agitation at 150 rpm. To harvest the cells, the 16 h growth culture was centrifuged at 10,000 rpm for 5 minutes followed by rinses using phosphate buffered saline (pH = 7.4, Sigma Aldrich) to remove excess media. The bacterial pellets were re-suspended in PBS with 0.5 optical density at 600 nm (OD600) which corresponded to  $\sim 5 \times 10^8$  colony forming units per milliliter (CFU/mL). Fluorescent bacteria viability tests were conducted using LIVE/DEAD BacLight bacterial viability kit (Invitrogen), which included SYTO 9 and propidium iodide (PI) dyes [28]. We note that both stains are employed frequently in a single staining step for viability assay. In contrast, we adopted the sequential stain protocol to demonstrate green-to-red fluorescence color change and the effectiveness of our approach. The results using sequential staining was identical to single staining. Precautions were taken to make sure no bacterial cells detached from the “sticky” glass slide (Superfrost Plus, VWR) during staining.

*Giardia lamblia* and *Cryptosporidium parvum* parasites were purchased in a mixed solution (AquaGlo A100FLR-1x, Waterborne Inc.) with  $\sim 10^5$  parasites/mL. Immunofluorescence identification of parasites was performed with antibody-conjugated fluorescein that selectively bind to membrane proteins present on *G. lamblia* and *C. parvum*.

### 2.7 Particle counting

Particle counting was performed in MATLAB. The images in each color channel were separately thresholded and binarized. Watershed was performed and an Otsu method of particle detection was used to count particles within the image [29].

## 3. Results

To demonstrate the optical performance along with the benefit of portability, we perform on-site microbiological imaging and detection with the smartphone microscope. In general, the specimens were collected from aqueous samples. Water sampling and monitoring can indicate the ecological health of an aqueous environment and to verify the quality of a water source, and is particularly important for water safety near populated areas [30]. However, current methods either rely on expensive ruggedized field equipment, or require sample collection, storage, and transportation to a lab, which are prone to contamination and increased turnaround time. In the following, we present results obtained from a performance analysis of the system, and three general applications in investigative microscopy: autofluorescence, fluorescence stains, and immunofluorescence.

### 3.1 Performance

Fluorescence performance depends on sensor sensitivity, and the performance of camera color filter. The color filter pattern (generally a Bayer pattern) allocates two pixels for green for every one red and one blue pixel. Thus, green images show higher sensitivity and resolution than red or blue images. Figure 4 shows multi-color fluorescent beads images acquired by a desktop microscope (Olympus BX-51) at 100x (top row) and by our smartphone microscope (middle row) under different illumination conditions: (a) ambient light bright-field, (b) white LED dark-field scattering, (c) blue LED ( $\lambda_{LED} = 465$  nm) and green filter ( $\lambda_{CUT-ON} = 525$  nm), and (d) green LED ( $\lambda_{LED} = 520$  nm) and red filter ( $\lambda_{CUT-ON} = 625$  nm). All beads in images acquired by the desktop microscope were clearly resolved. For images taken by the smartphone microscope, individual beads cannot be resolved in the bright-field image due to strong background, however they can be resolved after image deconvolution in white light and green fluorescence channel. Individual beads cannot be clearly resolved in the red fluorescence image even after deconvolution because of the lower light sensitivity explained earlier. The maximum resolving power of the smartphone microscope was 2  $\mu\text{m}$  with deconvolution.

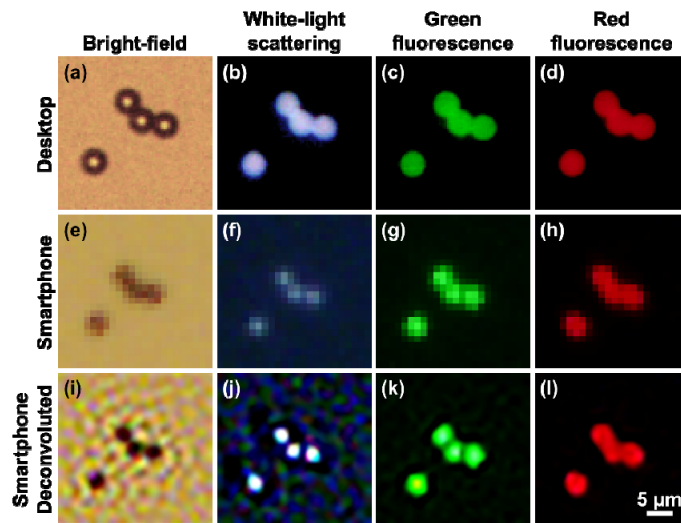


Fig. 4. Multi-color fluorescent beads imaged with: (top row) 100x desktop microscope, (middle row) smartphone microscope, and (bottom row) deconvoluted smartphone images.

### 3.2 Autofluorescence

Untreated water from a local detention pond (lat.  $29^{\circ}74'63$ , long.  $-95^{\circ}62'00$ ) was collected in a  $100\ \mu\text{m}$  volumetric glass slide for on-site imaging. All objects remained suspended in the water droplet during imaging. The LED illumination ensures wide incident angles and allows a portion of the TIR-guided light to couple into the water film and excite fluorescence from suspended *Spirogyra* algae with salient filamentous and helical structures [31]. The smartphone images with two different configurations are shown in Fig. 5. Scattering images were acquired with white light LED illumination without filters as shown in Fig. 5(a). The illumination provided true-color imaging of green *Spirogyra* algae in the dark-field mode. Various morphological structures of the algae including the cell wall and the characteristic helical pyron structures can be identified with a sample-to-background contrast of 0.82. The contrast is defined as  $I_{obj} / (I_{obj} + I_{bg})$ , where  $I_{obj}$  and  $I_{bg}$  are the respective intensities of the desired object and background. Magnified portions of the image are shown in Fig. 5(i)–5(iv) where it is noted that the scattered light arose from both the chlorophyll-rich helical structure and chlorophyll-free cell wall structures.

Fluorescence imaging was performed with blue LEDs ( $\lambda_{LED} = 465\ \text{nm}$ ) and a red filter ( $\lambda_{CUT-ON} = 600\ \text{nm}$ ) as shown in Fig. 5(b). The configuration was compatible with the fluorescence excitation / emission of chlorophyll (a, b) which has excitation peaks in the blue wavelength (430, 453 nm), and emission peaks in the red wavelength (662, 642 nm) [32]. The image contrast was found to be 0.45 due to light attenuation by the filter. However, the fluorescence imaging modality selectively highlights the chlorophyll-rich helical structures against the chlorophyll-free cell wall structures.

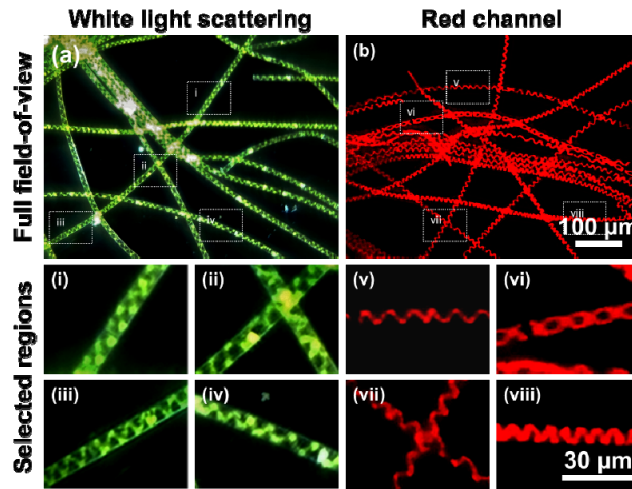


Fig. 5. Spirogyra algae imaged on-site with fluorescence smartphone microscope under (a) dark-field white light scattering, and (b) blue light excitation with red fluorescence emission modes. (i–viii). Selected regions for comparison.

### 3.3 Binding fluorescence stains

Bacterial viability studies are important for developing bacterial control procedures to limit bacterial infection [33], and to understand surface contamination and biofilm formation [34]. The development of fluorescent stains have enabled rapid imaging-based viability tests compared to conventional assays based on cell culture or metabolic characterization. Following standard staining protocols, two contrasting nucleic acid stains were used for bacterial viability tests: SYTO 9 (a green fluorophore) can penetrate both intact and compromised cell membranes, while propidium iodide (PI, a red fluorophore) can only penetrate compromised cell membranes. In other words, SYTO 9 stains all bacteria, live or dead, while PI only stains dead bacteria. The prepared samples were imaged by the smartphone with blue LED ( $\lambda_{LED} = 465$  nm) and green filter ( $\lambda_{CUT-ON} = 515$  nm) for SYTO 9, and with green LED ( $\lambda_{LED} = 520$  nm) and red filter ( $\lambda_{CUT-ON} = 625$  nm) for PI.

A particle counting algorithm based on intensity thresholding with watershed was used to obtain total bacteria as  $n_{all} = 885$  and  $n_{dead} = 54$ , or equivalently,  $n_{live} = 831$  (93.9%). Representative regions from the entire FOV are shown in Fig. 6, where (a, d) are from the green channel, (b, e) from the red channel, and (c, f) are the two channels overlaid. Proper sample dilutions are required to prevent aggregation which may cause incorrect counting. The full FOV image for bacterial binding fluorescence is shown in Fig. 7.

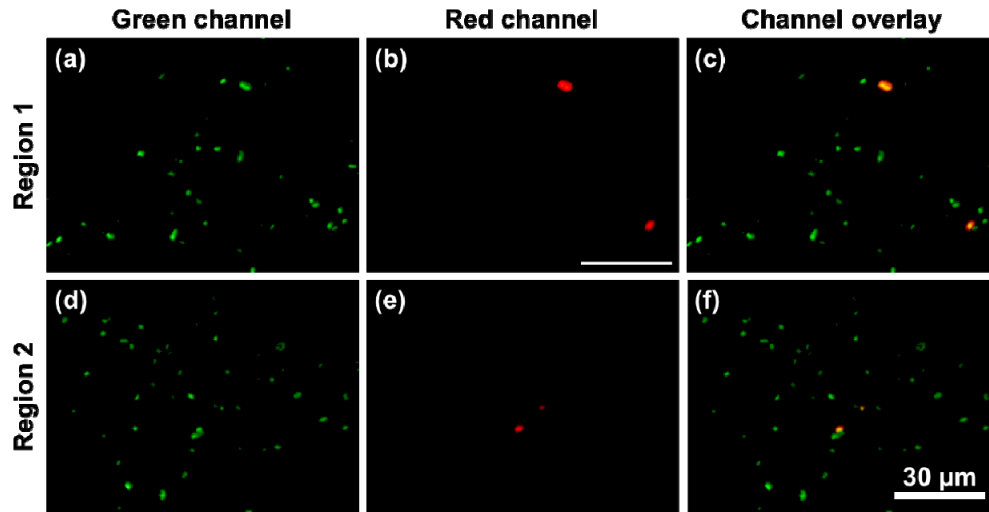


Fig. 6. Bacteria dried on glass seen under (left) green fluorescence, (center) red fluorescence, and (right) multi-color overlaid image. The multi-color full FOV image is shown in Fig. 7.

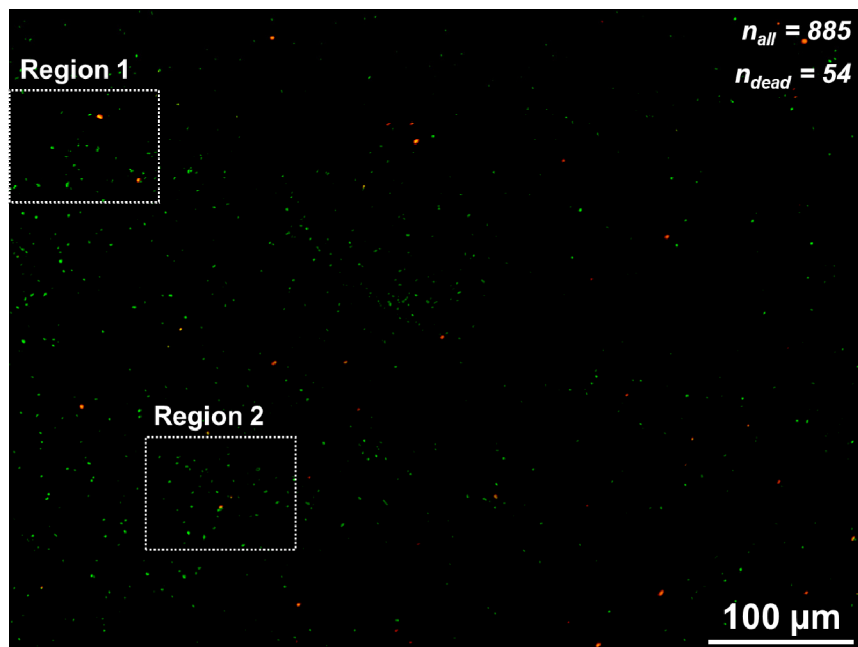


Fig. 7. Full FOV of multi-color fluorescence live/dead bacteria image. Selected regions of interest shown in Fig. 6.

### 3.4 Immunofluorescence

*Giardia lamblia* and *Cryptosporidium parvum* are waterborne parasites that cause gastroenteritis and are commonly found in public water bodies [35]. Frequent outbreaks of both highlight the importance of constant water monitoring procedures. Morphologically, *G. lamblia* is a larger oval-shaped parasite (8–13  $\mu\text{m}$   $\times$  7–10  $\mu\text{m}$ ), and *C. parvum* is a smaller circular parasite (5–7  $\mu\text{m}$ ). A mixture of both parasites and 6  $\mu\text{m}$  PS beads was dried on a glass slide. The PS beads were included as a potential confounding factor. The image obtained under bright-field shows mostly single particles in Fig. 8(a) and 8(c) (Color inverted

for comparison). To a trained pathologist, *G. lamblia* may be well distinguished from other background particles due to its large size. However, size-based analysis is prone to errors. For example, *C. parvum* parasites are virtually indistinguishable from polystyrene beads. The glass slide was subsequently immersed in an aqueous solution of antibody-conjugated-fluorescein that specifically binds to antigenic sites found only in *G. lamblia* and *C. parvum* membranes followed by DI water rinse. The high specificity of the immunofluorescence stain enabled the parasites to be identified in Fig. 8(b) and 8(d) without the interference of PS beads that appeared in Fig. 8(a) and 8(c). Parasites that are positioned side-by-side are not always identifiable with a smartphone bright-field image, but are clearly differentiable in the green fluorescence image either before (Fig. 8, circle 2) or after deconvolution (Fig. 8, circle 5). Furthermore, despite both parasites staining the same color, an EPA standard protocol exists to distinguish between the two parasites based on fluorescence imaging [36]. With the aid of cell counting algorithms, our approach can provide quick on-site detection and counting of parasites. The FOV image for parasites is shown in Fig. 9.

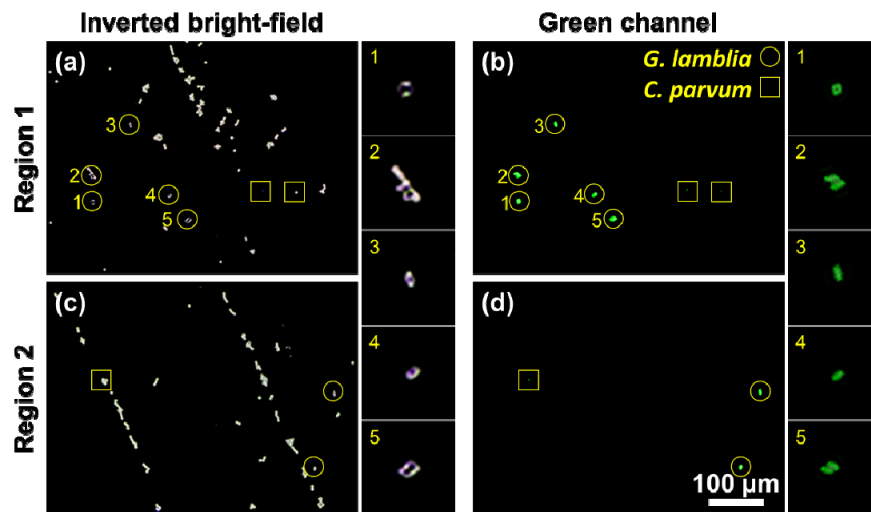


Fig. 8. *Giardia lamblia* and *Cryptosporidium parvum* mixed with 6  $\mu\text{m}$  polystyrene beads seen under (left) bright-field smartphone microscope and (right) green fluorescence. *G. lamblia* and *C. parvum* are respectively marked. The multi-color full FOV image is shown in Fig. 9.

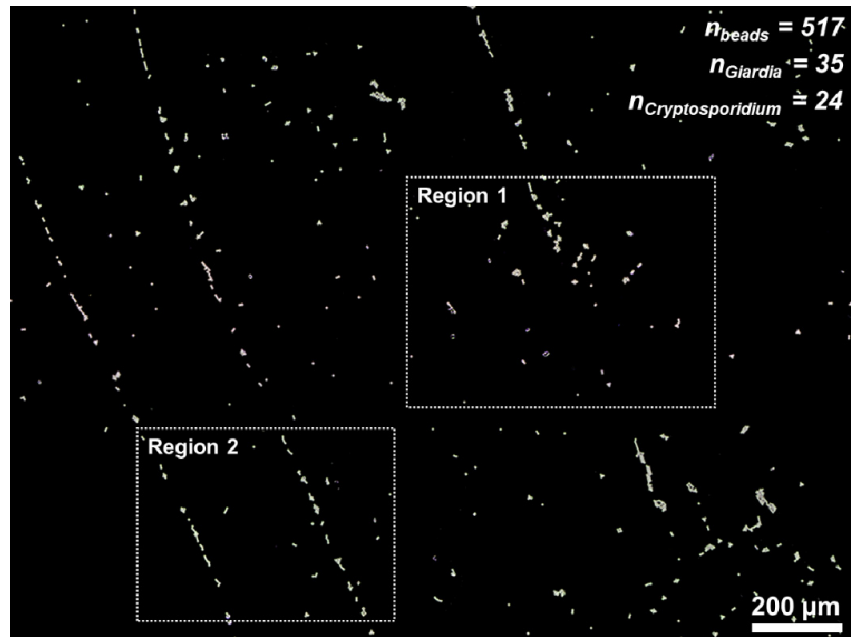


Fig. 9. Full FOV color-inverted bright-field image of parasites mixed with polystyrene beads with selected regions of interest shown in Fig. 8.

#### 4. Conclusion

Fluorescence microscopy is a powerful tool in cellular and microbiological investigations, but has been limited to laboratory use due to the lack of simple portable setups. Although recent developments in smartphone microscopy have made significant stride, existing embodiments only have moderate adoption due to various technical challenges. To overcome this barrier, we have developed a multi-color fluorescence smartphone microscope for three common tasks in investigative fluorescence microscopy: autofluorescence, fluorescent stains, and immunofluorescence. We have integrated a single add-on lens and slide-launched, TIR-guided illumination with an entry-level phone, which mimics the general smartphone offerings in developing countries where such a device may have its greatest impact. Furthermore, the modular, 3D-printed design ensures universal device compatibility, and the orthogonal illumination and imaging angles ensure that the setup can be compatible with different lenses. With this device, we have obtained autofluorescence images from chlorophyll in algae for microstructural observations, binding fluorescence of cell viability stains to monitor bacterial growth on a nonporous surface, and immunofluorescence identification of *Giardia lamblia* and *Cryptosporidium parvum* waterborne parasites. The lightweight (<27 g), low cost (<\$20), and open-source 3D-printed modules have the potential to promote do-it-yourself fluorescence microscopy.

#### Acknowledgement

This research was partially supported by National Science Foundation (NSF) CBET-1643391. The authors acknowledge Hang Nguyen for cell staining and Dr. David Mayerich for access to a fluorescence microscope.

#### Disclosures

YS, WS: Dr. Shih LLC (I, P).